Korean J. Chem. Eng., 33(2), 539-546 (2016)
DOI: 10.1007/s11814-015-0160-5

pISSN: 0256-1115
eISSN: 1975-7220

Photocatalytic degradation of azo dye using nano-ZrO_2/UV/Persulfate: Response surface modeling and optimization

Mahsa Moradi[*,], Farshid Ghanbari[***,†], Mohammad Manshouri[****], and Kambiz Ahmadi Angali[*****]**

*Department of Environmental Health Engineering, School of Paramedicine and Public Health, Semnan University of Medical Sciences, Semnan, Iran
**Department of Environmental Health Engineering, School of Medical Sciences, Tarbiat Modares University, Tehran, Iran
***Department of Environmental Health Engineering, School of Public Health, Ahvaz Jundishapur University of Medical Sciences, Ahvaz, Iran
****Department of Environmental Health Engineering, School of Public Health, Shahid Beheshti University of Medical Sciences, Tehran, Iran
*****Department of Statistics and Epidemiology, Ahvaz Jundishapur University of Medical Sciences, Ahvaz, Iran
(*Received 11 January 2015 • accepted 27 July 2015*)

Abstract−Dyes have always been considered in the context of recalcitrant organic pollutants in water. The present research has focused on the decolorization of Direct Blue 71 (DB71) using photocatalysis process of nano-ZrO_2/UV/Persulfate. Response surface method with central composite design was applied to determine the effects of four main factors (time, ZrO_2 dosage, persulfate dosage and pH) on decolorization of DB71. The results indicated that the obtained quadratic model had a high R-squared coefficient based on the analysis of variance (ANOVA). Time had the highest effect (45.5%) on decolorization of DB71. The optimum condition predicted for complete decolorization was pH=7, 0.4 g ZrO_2, 0.75 mM persulfate and 40 min reaction time. Verification experiments confirmed that there was good agreement between the experimental and predicted responses. The studied photocatalytic process could oxidize and destruct the structure of the DB71, and average oxidation state (AOS) significantly increased from −1.5 to +1.33, indicating the presence of more oxidized by-products and, consequently, improvement of biodegradability. The quenching tests showed that sulfate radical was the major agent in DB71 decolorization. It can be concluded that nano-ZrO_2/UV/Persulfate is a very effective process for decolorization of colored wastewater.

Keywords: Nano-ZrO_2, Synthetic Dye, Sulfate Radical, Response Surface Method

INTRODUCTION

Dyes have long been used in dyeing, textiles, plastics, cosmetics and food industries. It is estimated that 10-15% of the dyes are lost during the dyeing process entering the effluents [1]. Some dyes and their precursors are suspected to be human carcinogens as they form toxic aromatic amines [2]. Dyes have complicated molecular structures and therefore their biodegradation is difficult [3,4]. There are conventional processes for the removal of dyes from contaminated water including coagulation, adsorption and membrane processes. These processes cannot destruct organic compounds and can merely separate dyes from the effluent and, consequently, concentrate them within the sludge [5]. Advanced oxidation processes (AOPs) have been proven to be one of the most effective treatments for wastewaters that are difficult to treat biologically. In general, AOPs are based on generation of highly reactive radicals (especially hydroxyl radicals) in sufficient quantity for the degradation of organic compounds [6,7]. Among AOPs, the photocatalysis process is likely to be the most popular process. In photocatalysis, a semiconductor is irradiated with UV source; an electron is excited from the valence bond to the conduction bond (e^-) leaving a hole in the valence bond (h^+) [8,9].

$$\text{Semiconductor} + \text{UV} \rightarrow e^- + h^+ \quad (1)$$

Several UV/semiconductor systems have been used for the photocatalytic degradation of organic pollutants, including TiO_2, ZnO, WO_3, ZrO_2 and Fe_2O_3 [8]. The photogenerated hole reacts with hydroxyl ion to produce hydroxyl radical which is a strong oxidant with E^0=2.7 V (Eqs. (2) and (3)). Hydroxyl radical can destroy organic compounds converting them to mineral compounds [10].

$$h^+ + OH^- \rightarrow HO^\bullet \quad (2)$$

The rate and efficiency of photocatalysis process can be reduced when the photogenerated holes and electrons are recombined. To prevent recombination of electron with hole, an electron acceptor should be provided. Oxygen is the most common electron acceptor that can react with photogenerated electron producing superoxide radical ($O_2^{-\bullet}$) [11].

$$O_2 + e_{CB}^- \rightarrow O_2^{\bullet -} \quad (3)$$

†To whom correspondence should be addressed.
E-mail: ghanbari.env@gmail.com

Alternatively, the presence of oxidants as electron acceptors can significantly improve the efficiency of the photocatalysis process [12]. Moreover, addition of an oxidant enhances the generation of reactive radical species, especially in case of application of hydrogen peroxide and persulfate. Persulfate (PS) is a strong oxidant with E^0=2.01 V, which is superior due to its stability, low cost, ease of storage and high solubility [12,13]. More recently, sulfate radical based AOPs have been studied to degrade various pollutants. Apart from the fact that persulfate is an electron acceptor for photocatalysis reactions, it can be a source for production of sulfate radicals in condition that UV is used as an activator. In fact, persulfate can be activated through both absorption of conduction bond electron and UV irradiation (Eqs. (4) and (5)) [12,14].

$$S_2O_8^{2-} + e_{CB}^- \rightarrow SO_4^{2-} + SO_4^{\bullet -} \quad (4)$$

$$S_2O_8^{2-} + UV \rightarrow SO_4^{\bullet -} + SO_4^{\bullet -} \quad (5)$$

The produced sulfate radical is an efficient oxidant (E^0=2.6-3.1 V), having a higher life time in comparison with the hydroxyl radical [15]. Good performance of UV/PS has been reported for treatment of various pollutants [16,17], whereas, the application of PS in UV/semiconductor systems (photocatalysis) has been rarely considered. In this study, ZrO_2 nanoparticle was used as the semiconductor. Actually, few investigations have been carried out to determine efficiency of ZrO_2 in such systems. Although TiO_2/UV/PS system has been studied for various compounds, the nano-ZrO_2/UV/PS system has not been investigated yet.

In this study, we evaluated the performance of nano-ZrO_2/UV/PS system in decolorization of Direct Blue 71 (DB71) as a sample dye with a complex molecular structure and azo bond. Optimization of photocatalysis process in presence of various PS dosages has not been reported in literature. Hence, to determine the optimal condition, response surface method was applied for nano-ZrO_2/UV/PS system for decolorization of DB71. Finally, identification of reaction mechanism was evaluated by quenching experiments.

MATERIALS AND METHODS

1. Materials and Reagents

Direct blue 71 dye was supplied from Alvan Sabet Company (Iran) and its characteristics are given in Table 1. Sodium persulfate ($Na_2S_2O_8$) and sodium hydroxide (NaOH) were purchased from Fluka Inc. Zirconyl chloride octahydrate ($ZrOCl_2 \cdot 8H_2O$) and ammonia hydroxide (NH_4OH-28%) were provided from Sigma-Aldrich Company. Ethanol and tert-butyl alcohol were purchased from Alfa Aesar Company.

Table 1. Characteristics of direct blue 71

Dye	Direct blue 71
Structure	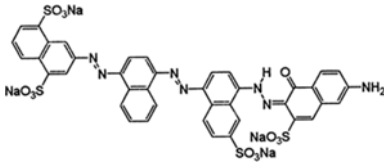
Chemical formula	$C_{40}H_{23}N_7Na_4O_{13}S_4$
Color Index No.	34140
Molecular weight (g/mol)	1029
CAS No.	4399-55-7

2. Preparation of ZrO_2 Nanoparticle

Zirconia nanoparticle was synthesized by precipitation method. In this way, a solution of 0.1 M $ZrOCl_2 \cdot 8H_2O$ was hydrolyzed by drop-wise addition of ammonia hydroxide. Meanwhile, the solution was continually stirred by magnetic stirrer until solution pH of 10.5 was achieved. The obtained precipitate ($Zr(OH)_4$) was washed with distilled water until all chloride ions were removed. The presence of Cl^- was checked by silver nitrate. Finally, the precipitates were dried in an oven at 110 °C for 12 h and then calcined at 600 °C for 4 h [18].

3. Photocatalysis Experiments

All experiments were performed in a batch system. Photocatalysis experiments were carried out in a cylindrical quartz reactor with 5 cm diameter and 15 cm height. UV irradiation was provided by four UVC lamps (6 W-Osram with maximum irradiation at 254 nm) which were placed around the reactor to avoid rising of the temperature. Photocatalytic degradation of 200 mL DB71 solution with a concentration of 50 mg/L (This concentration was constant in all experiments) was evaluated at various pH levels, reaction times, ZrO_2 and PS dosages according to design of experiments that is brought in Table 2. The solution pH was adjusted by 0.1 N H_2SO_4 and NaOH while solution was magnetically stirred. The temperature of solution did not exceed 27 °C using two fans. The samples were taken at final reaction time in each experiment.

4. Experimental Design

RSM is a statistical tool that can quantify the relationship between independent variables and responses. Amongst RSM designs, central composite design (CCD) is the most applicable method for optimization of water and wastewater processes. In this study, CCD was used to optimize nano-ZrO_2/UV/PS for decolorization of DB71. Four factors at five levels were chosen to evaluate the influence of operational parameters on the decolorization efficiency of DB71. The variables included ZrO_2 dosage, pH, reaction time and PS concentration (Table 2). In all, 31 experiments were utilized including 16 factorial points (α=±1), 8 axial points (α=±2) and 7 replications at the center point (α=0).

The effects of independent variables on decolorization (Y) were analyzed based on a quadratic equation model as given in Eq. (6).

$$Y = b_0 + \sum b_i X_i + \sum b_{ii} X_i X_i + \sum b_{ij} X_i X_{ij} + \varepsilon \quad (6)$$

where, Y is the predicted value of the response, b_0 is constant, b_i is the slope of the factor x_i (i=1, 2, 3 and 4), b_{ii} is the regression coef-

Table 2. Level of independent variables and experimental range

Variables	Levels				
	−2	−1	0	1+	2+
ZrO_2 (g/L), X_1	0.2	0.4	0.6	0.8	1
PS (mM), X_2	0.2	0.4	0.6	0.8	1
Time (min), X_3	10	20	30	40	50
pH, X_4	3	5	7	9	11

ficient for squared effects, b_{ij} is the interaction coefficient and ε is the residual term [19].

5. Analytical Methods

DB71 concentration was measured by UV-visible spectrophotometer (Hach, DR5000) at wavelength of 587 nm, which is the wavelength of maximum absorption. Total organic carbon (TOC) measurements were performed by TOC analyzer (Shimadzu-V_{CSH}, Japan). Chemical oxygen demand (COD) values were measured by colorimetric method based on the Standard Methods [20]. Average oxidation state (AOS) value was calculated based on Eq. (7) [21,22].

$$AOS = 4 - 1.5\frac{COD}{TOC} \tag{7}$$

where AOS values are between −4 and +4 for methane and carbon dioxide, respectively.

X-ray diffraction measurement was recorded by a D8 Bruker Advanced diffractometer with Cu-Kα radiation. The morphology and structure of ZrO_2 nanoparticle were characterized by scanning electron microscope (SEM) (Hitachi model S-3000H, Japan). FTIR spectra of ZrO_2 nanoparticle were recorded by using a Vertex 70 spectrophotometer (Bruker, Germany) with a resolution of 4 cm^{-1}.

RESULTS AND DISCUSSION

1. Characteristics of ZrO_2 Nanoparticle

Fig. 1 shows characteristics of nano-ZrO_2 particles. Fig. 1(a) displays XRD patterns of the produced nanoparticle. As can be seen, the main phase of the sample is zirconia (ZrO_2), which is indicated by two main peaks at diffraction angles 2θ of 28.15° and 31.47°. Both peaks represent plane orientations in the crystals of (−111) and (111), respectively. The average crystalline size of ZrO_2 was calculated based on Debye–Scherrer formula (Eq. (8)) [23]:

$$D = \frac{0.9\lambda}{\beta\cos\theta} \tag{8}$$

where D is the average crystallite size, λ is the wavelength of the X-ray radiation (0.1541 nm), β is the full width at half maximum (fwhm) intensity of the peak and θ is the diffraction angle.

The mean size of the produced nanoparticles is approximately 75 nanometers. This range of size provides high surface area and, consequently, high adsorption of dye for photocatalytic degradation. Fig. 1(b) presents SEM image of nano-ZrO_2. The morphology of nano-ZrO_2 surface was characterized by SEM image. Fig. 1(c) displays spectra obtained by means of FTIR analysis of the nano-

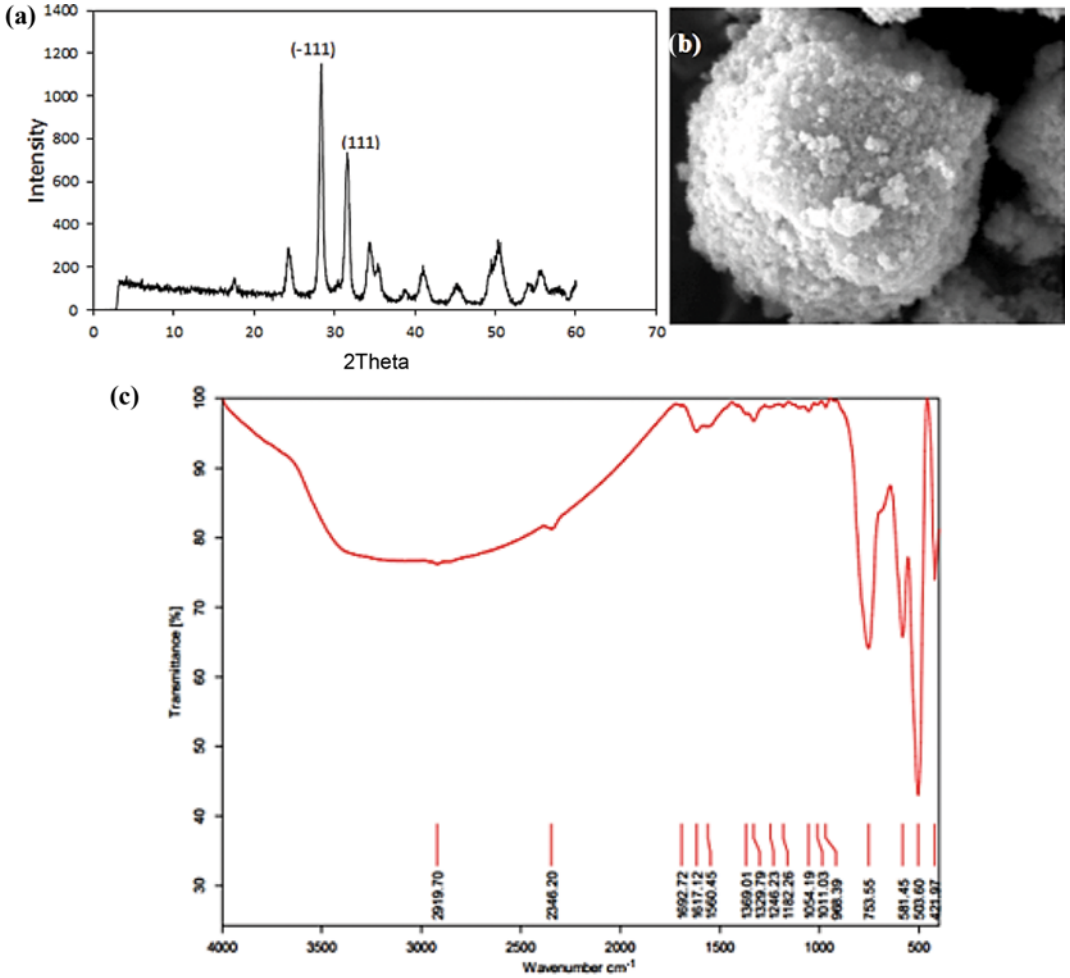

Fig. 1. (a) XRD analysis of nano-ZrO_2 (b) SEM image of nano-ZrO_2 (c) FTIR spectrum of nano-ZrO_2.

Table 3. Experimental design and results obtained for DB71 removal efficiency

Runs	ZrO_2 (g/L)	PS (mM)	Time (min)	pH	Decolorization (%)	Decolorization (%)
					Actual	Predicted
1	0.6	0.6	30	7	80.2	80.86
2	0.4	0.8	40	9	100.0	101.50
3	0.6	0.6	10	7	61.2	61.63
4	0.4	0.4	40	9	80.9	76.72
5	0.6	0.6	30	7	78.9	80.86
6	0.8	0.8	20	5	70.1	75.84
7	0.2	0.6	30	7	77.3	80.57
8	0.8	0.4	20	5	73.2	67.15
9	0.8	0.8	20	9	75.6	72.65
10	0.4	0.4	40	5	70.5	68.90
11	0.8	0.4	20	9	61.2	64.32
12	0.4	0.8	20	9	75.6	72.89
13	0.8	0.8	40	5	100.0	95.70
14	0.6	0.6	50	7	100.0	102.56
15	0.8	0.8	40	9	100.0	100.92
16	0.6	1.0	30	7	100.0	100.87
17	1.0	0.6	30	7	91.2	90.91
18	0.6	0.6	30	7	81.6	80.86
19	0.4	0.4	20	9	55.9	55.65
20	0.6	0.6	30	3	55.3	55.92
21	0.6	0.6	30	11	58.2	60.56
22	0.6	0.2	30	7	65.3	67.40
23	0.6	0.6	30	7	82.0	80.86
24	0.6	0.6	30	7	81.6	80.86
25	0.6	0.6	30	7	80.4	80.86
26	0.4	0.8	40	5	95.6	94.04
27	0.4	0.8	20	5	75.2	73.82
28	0.8	0.4	40	5	75.2	79.47
29	0.4	0.4	20	5	55.6	56.23
30	0.6	0.6	30	7	81.3	80.85
31	0.8	0.4	40	9	88.2	85.03

ZrO_2. The most significant features of the FTIR spectra of nano-ZrO_2 are recorded in the range of 4,000-400 cm^{-1}. The peaks of 421, 503 and 571 cm^{-1} can be related to Zr-O-Zr bond. These sharp peaks reveal that the precipitation method is effective for formation of zirconia.

2. Statistical Analysis and Model Fitting

Experimental and predicted values obtained for decolorization of DB71 at the design points are presented in Table 3. Statistical analysis of the model was performed to evaluate the analysis of variance (ANOVA), indicating F-value of 31.48 and R^2=0.965, implying that the model was statistically significant (Table 4) [24]. The corresponding R-squared value indicates that 96.5% of the variability for DB71 removal can be explained by the regression model, while merely 3.5% of the response variability cannot be explained through the obtained model. Moreover, the adjusted R-squared is very close to the R-squared value (0.934-0.965) as another evidence for goodness of the model fit [25,26]. Table 4 also shows that linear and square parameters are significant with P-values<0.01, while interaction parameter has F-value 2.75 with P-value 0.049. In addition, the computed F-value (31.48) is much greater than the tabu-

Table 4. Analysis of variance for quadratic model using central composite design

Source	DB71 removal				
	SS	DF	MS	F-value	P-value
Regression	5664.89	14	404.63	31.48	0.000
Linear	4385.7	4	1096.43	85.3	0.000
Square	1067.11	4	266.78	20.76	0.000
Interaction	212.08	6	35.35	2.75	0.049
Residuals	205.65	16	1285		
Lack-of-fit	198.57	10	19.86		
Pure error	7.08	6	1.18		
Total	5870.54	30			
R^2=0.965	**R^2_{adj}=0.934**				

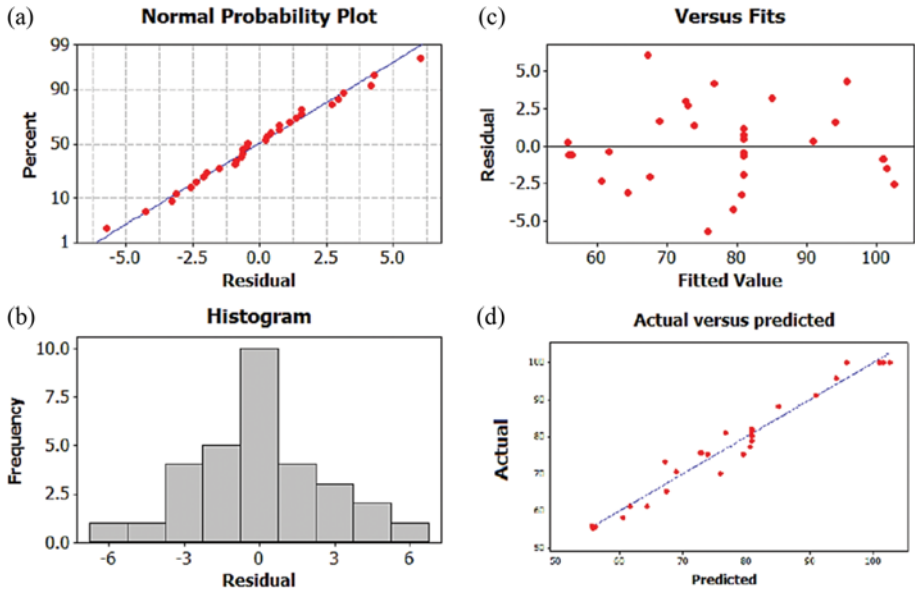

Fig. 2. Residual plots (a)-(c) of UV/ZrO_2/Persulfate systems for DB71 removal (d) Plot of the actual and predicted values.

lar F-value that equals with 3.45 ($F_{0.01(14,16)}$), revealing that the efficiency differences are significant [27].

The adequacy of the model was also evaluated by plotting distribution of residuals. The straight line in Fig. 2(a) shows that residuals have normal distribution. Likewise, Fig. 2(b) depicts a plot of observed residuals versus their frequency, confirming that residuals distribution is in good agreement with the normal distribution (histogram graph). Fig. 2(c) plots residuals against the fitted values. Approximately half of the residuals are above and another half are below the zero line, displaying that mean of residuals is close to zero. Fig. 2(a)-(c) emphasizes normal distribution of residuals and adequacy of the model [28,29]. Fig. 2(d) depicts diagnostic plot of actual values versus the predicted ones: the obtained points lay adjacent to diagnostic line, indicating model suitability [30].

Table 5. Estimated regression coefficients and corresponding t and P-values for DB71 removal

Model	Coefficient (b)	SE coefficient	T-value	P-value
Constant	80.85	1.35	59.67	0.000
X_1	2.58	0.73	3.53	0.003
X_2	8.36	0.73	11.98	0.000
X_3	10.22	0.73	13.98	0.000
X_4	1.15	0.73	1.58	0.133
X_1^2	1.22	0.67	1.82	0.087
X_2^2	0.82	0.67	1.22	0.238
X_3^2	0.30	0.67	0.46	0.651
X_4^2	−5.65	0.67	−8.43	0.000
X_1X_2	−2.22	0.89	−2.48	0.025
X_1X_3	−0.087	0.89	−0.098	0.925
X_1X_4	−0.56	0.89	−0.628	0.539
X_2X_3	1.887	0.89	2.10	0.051
X_2X_4	−0.087	0.89	−0.098	0.923
X_3X_4	2.1	0.89	2.34	0.032

3. Analysis of DB71 Removal

According to the results, an empirical model (Eq. (9)) is presented, which shows the relationship between the response and the factors (independent variables) in terms of coded factors.

$$Y_1=80.85+2.58X_1+8.36X_2+10.23X_3+1.15X_4+1.22X_1^2 +0.82X_2^2+0.3X_3^2-5.65X_4^2-2.22X_1X_2-0.087X_1X_3 -0.56X_1X_4+1.88X_2X_3-0.087X_2X_4+2.1X_3X_4 \quad (9)$$

The significant variables of this model were identified by Student t-test and P-value. Regression coefficients, t-values (b/SE coefficient) and P-values are given in Table 5. Smaller P-value along with larger t-value indicates more significance of the regression coefficient. Pareto chart was also used to identify the contribution of each factor. It was applied for ease of interpretation of the results by which the percentage effect of each factor on the response was calculated based on the following equation [29,31]:

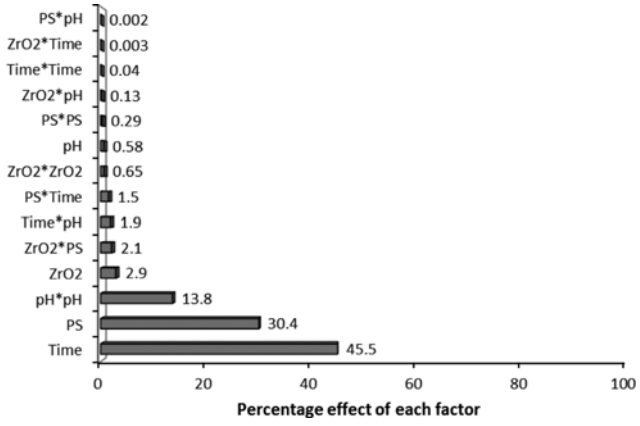

Fig. 3. Pareto chart for decolorization of direct blue 71 by nano-ZrO_2/UV/PS.

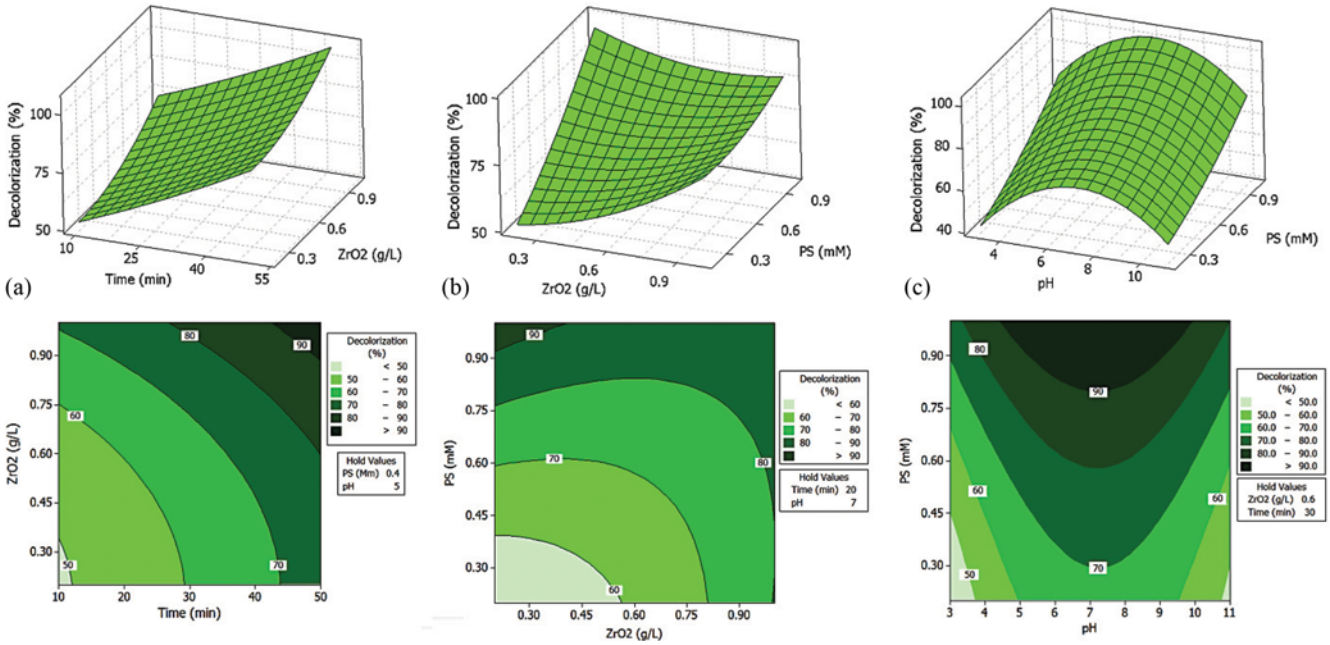

Fig. 4. Contour and surface plots of nano-ZrO_2/UV/PS systems (a) ZrO_2 dosage versus time (b) PS versus ZrO_2 dosages (c) PS dosages versus pH.

$$P_i = \left(\frac{b_i^2}{\sum b_i^2}\right) \times 100 \qquad (i \neq 0) \qquad (10)$$

where, b represents related regression coefficient of the parameter. In Fig. 2, the Pareto chart illustrates percentage effects of the influential parameters in DB71 removal by nano-ZrO_2/UV/PS system. As can been seen in Fig. 3, amongst the variables, variable of time (45.5%), variable of persulfate (30.4%) and square of pH (13.8%) have had the highest effects on DB71 removal efficiency by the studied photo-oxidative process.

4. Response Surface and Contour Plots

The two- and three-dimensional plots were used to represent combined effects of two factors for the prediction of DB71 removal. Fig. 4(a) displays response surface and contour plots indicating decolorization (%) as a function of ZrO_2 dosage and time. As can be seen, with increase of time, decolorization increased markedly, whereas increase of ZrO_2 dose had lower influence in comparison with the time variable. In general, irradiation time has been the most influential factor in the nano-ZrO_2/UV/PS system.

Fig. 4(b) shows the combined effects of PS concentration and ZrO_2 dosage on DB71 removal efficiency. It is obvious that increase in oxidant concentration and semiconductor dosage has improved DB71 removal efficiency, since additional sulfate and hydroxyl radicals have been provided through photo-excitation of ZrO_2, photolysis of persulfate and scavenging of conduction bond electrons by persulfate. These free radicals can react with dye molecule and destroy its organic structure consequently. As shown in Fig. 4(b), in PS concentrations of higher than 0.8 mM, more than 80% removal efficiency was provided, regardless of increasing ZrO_2 dosage. As illustrated in the Pareto chart, PS concentration had higher influence on decolorization efficiency in comparison with the ZrO_2 dosage.

Fig. 4(c) shows the effect of PS concentration and pH on decolorization efficiency in 30 min reaction time and ZrO_2 dosage of 0.6 g/L. As illustrated, a funnel appears in the contour plot that its end faces pH of 7. In fact, highest removal efficiency occurred at pH of 7, although at pH range of 5-9, adequate removal efficiency was obtained resulting from appropriate performance of persulfate in a wide range of pH. The suitable performance at wide pH range is one of the reasons that persulfate has been preferred to hydrogen peroxide [32]. When the PS concentration increased from 0.3 to 0.9 mM, decolorization efficiency increased from about 50% to >90%.

5. Optimization and Validation

To optimize nano-ZrO_2/UV/PS system, response optimizer was utilized. The highest efficiency (complete decolorization) was defined as the favorable target. The optimum values of independent variables (PS concentration, ZrO_2 dosage, time and pH) for complete decolorization are presented in Table 6. To confirm the reliability of the model, three experiments were conducted in optimum conditions and the obtained results are in Table 6. The results show that there was good agreement between the predicted and experimental values of the response, confirming the validity of the model. Saien and Soleymani [33] reported that 97% decolorization of DB71 was obtained under conditions of 120 min reaction time, natural pH and 40 mg/L TiO_2, which is in agreement with the present study [33]. Song et al. [34] stated that photocatalysis process with TiO_2 can completely degrade Direct Blue 78 in presence of sunlight under

Table 6. Optimal condition for 100% decolorization and results of verification experiments

	ZrO_2 (g/L)	PS (mM)	Time (min)	pH	Verification experiments-decolorization (%)
Run	0.4	0.75	40	7	97.1%±1.7

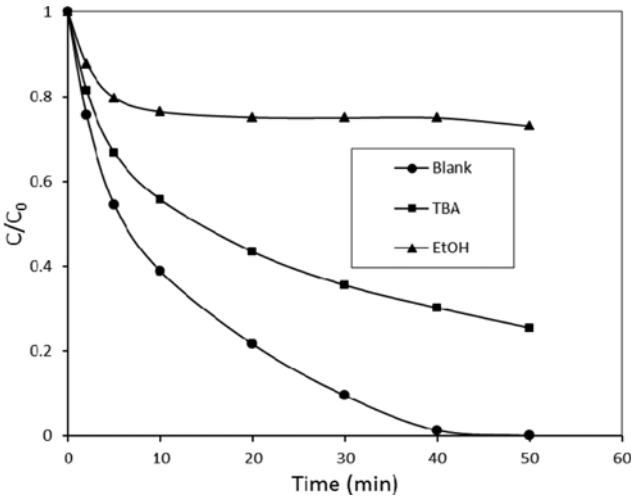

Fig. 5. Decolorization of DB71 in presence of ethanol and tert-butyl alcohol.

conditions of 6 h irradiation time, pH=3 and dosage of TiO_2 1.0 g/L [34]. Another study (2013) showed that N-TiO_2 could decolorize almost 100% Acid Blue 25 at pH=3 in an hour [35]. In comparison with these studies, the present study has a shorter reaction time which, can be an important advantage.

6. Identification of the Reaction Mechanism

To determine the major reactive radical species, quenching tests were carried out using ethanol (EtOH) and tert-butyl alcohol (TBA) as scavenging agents. EtOH can effectively scavenge both $HO^{\bullet}$ and $SO_4^{\bullet-}$ while TBA scavenges $HO^{\bullet}$ with high reaction rate [36-38]. Fig. 5 demonstrates the effect of EtOH (50 mM) and TBA (50 mM) on DB71 decolorization. The results clearly indicated that in presence of EtOH, decolorization significantly decreased. This result represents that the mechanism of the system has been based on generation of the radicals. On the other hand, in presence of TBA, decolorization decreased to 74.5% in 50 min reaction time, while complete decolorization was obtained in blank condition (without scavenging agents). This relative reduction in decolorization results from the presence of more sulfate radicals since hydroxyl radical was scavenged with TBA. Hence, it can be deduced that major radical in the system has been the sulfate radical that could degrade DB71 in presence of TBA.

7. Mineralization of DB71

Dye degradation degree was evaluated through measurements of TOC, COD and average oxidation state (AOS) parameters in optimum condition.

The results of TOC and COD removals are shown in Fig. 6(a): 45.6% TOC removal was achieved during 80 min reaction time. After that, TOC removal efficiency did not considerably change. It is supposed to be attributed to the presence of organic intermediates with difficult mineralization potential. In case of COD, removal efficiency increased during 100 min reaction time in a way that 71.6% reduction was observed. In fact, COD reduction has been much more than TOC reduction in this system, which is similar to some other studies [39,40].

Fig. 6(b) shows AOS variation trend during 140 min reaction time. As can be seen, the solution containing 50 mg/L DB71 is relatively non-biodegradable and toxic with an AOS value of −1.5. In spite of that, the photocatalytic process along with persulfate increased the AOS value significantly. After the oxidation process, AOS values changed from negative values to positive values and in 140 min reached its maximum value which was +1.33. These results definitely indicate that the produced by-products have adequately been oxidized and biodegradability has been improved indirectly [21,30].

CONCLUSION

We investigated the performance of nano-ZrO_2/UV/persulfate system for decolorization of Direct Blue 71. Response surface method was used for modeling and analysis of independent variables having influence on decolorization. The quadratic model had high R-squared coefficient (0.965) and high F-value, confirming that the model was valid to predict the experimental results. The Pareto analysis showed that reaction time was the most influential factor with 45.5% effect. The optimum condition predicted for complete decolorization (100%) was pH=7, 40 min reaction time, 0.4 g ZrO_2 and 0.75 mM persulfate. AOS value as a mineralization index increased markedly during photocatalysis/persulfate process at obtained optimum condition. Finally, the results confirmed that RSM was a beneficial tool to optimize the photocatalysis/persulfate system.

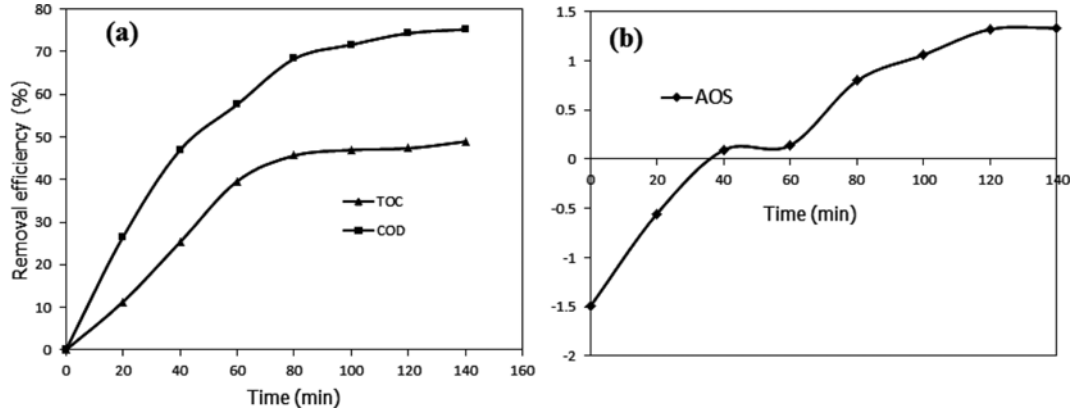

Fig. 6. (a) TOC and COD removals of DB71 at optimum condition (b) AOS value versus reaction time.

Thus, the nano-ZrO_2/UV/persulfate system is a very effective oxidative process for organic pollutant degradation.

ACKNOWLEDGEMENT

Authors are thankful to Mrs. Rajabi and Ms. Omidinasab for assistance in some tests.

REFERENCES

1. E. Chatzisymeon, N. P. Xekoukoulotakis, A. Coz, N. Kalogerakis and D. Mantzavinos, *J. Hazard. Mater.*, **137**, 998 (2006).
2. X.-R. Xu and X.-Z. Li, *Sep. Purif. Technol.*, **72**, 105 (2010).
3. F. E. Fernades Rêgo, A. M. Sales Solano, I. C. da Costa Soares, D. R. da Silva, C. A. Martinez Huitle and M. Panizza, *J. Environ. Chem. Eng.*, **2**, 875 (2014).
4. F. Ghanbari and M. Moradi, *J. Environ. Chem. Eng.*, **3**, 499 (2015).
5. A. Eslami, M. Moradi, F. Ghanbari and F. Mehdipour, *J. Environ. Health Sci. Eng.*, **11**, 1 (2013).
6. V. Augugliaro, M. Litter, L. Palmisano and J. Soria, *J. Photochem. Photobiol., C*, **7**, 127 (2006).
7. A. Yazdanbakhsh, F. Mehdipour, A. Eslami, H. S. Maleksari and F. Ghanbari, *Water Sci. Technol.*, **71**, 1097 (2015).
8. M. N. Chong, B. Jin, C. W. K. Chow and C. Saint, *Water Res.*, **44**, 2997 (2010).
9. M. R. Hoffmann, S. T. Martin, W. Choi and D. W. Bahnemann, *Chem. Rev.*, **95**, 69 (1995).
10. U. I. Gaya and A. H. Abdullah, *J. Photochem. Photobiol., C*, **9**, 1 (2008).
11. B. Gözmen, *Environ. Prog. Sustain. Energy*, **31**, 296 (2012).
12. R. Hazime, Q. H. Nguyen, C. Ferronato, A. Salvador, F. Jaber and J. M. Chovelon, *Appl. Catal., B*, **144**, 286 (2014).
13. Y. F. Rao, L. Qu, H. Yang and W. Chu, *J. Hazard. Mater.*, **268**, 23 (2014).
14. S. Moghaddam, M. Rasoulifard, M. Vahedpour and M. Eskandarian, *Korean J. Chem. Eng.*, **31**, 1577 (2014).
15. K. Govindan, M. Raja, M. Noel and E. J. James, *J. Hazard. Mater.*, **272**, 42 (2014).
16. Y.-T. Lin, C. Liang and J.-H. Chen, *Chemosphere*, **82**, 1168 (2011).
17. H. Eskandarloo, A. Badiei and M. A. Behnajady, *Desal. Water Treat.*, 1 (2014).
18. B. Tyagi, K. Sidhpuria, B. Shaik and R. V. Jasra, *Ind. Eng. Chem. Res.*, **45**, 8643 (2006).
19. A. T. Nair, A. R. Makwana and M. M. Ahammed, *Water Sci. Technol.*, **69**, 464 (2014).
20. APHA, *Standard methods for the examination of water and wastewater*, APHA, Washington DC (1999).
21. L.-A. Lu, Y.-S. Ma, M. Kumar and J.-G. Lin, *Sep. Purif. Technol.*, **81**, 325 (2011).
22. P. Kajitvichyanukul and N. Suntronvipart, *J. Hazard. Mater.*, **138**, 384 (2006).
23. R. Y. Hong, J. H. Li, L. L. Chen, D. Q. Liu, H. Z. Li, Y. Zheng and J. Ding, *Powder Technol.*, **189**, 426 (2009).
24. F. Torrades and J. García-Montaño, *Dyes Pigm.*, **100**, 184 (2014).
25. R. Davarnejad, M. Mohammadi and A. F. Ismail, *J. Water Proc. Eng.*, **3**, 18 (2014).
26. S. Chun, S. An, S. Lee, J. Kim and S. Chang, *Korean J. Chem. Eng.*, **31**, 994 (2014).
27. F. Rasouli, S. Aber, D. Salari and A. R. Khataee, *Appl. Clay Sci.*, **87**, 228 (2014).
28. K. Cruz-González, O. Torres-Lopez, A. M. García-León, E. Brillas, A. Hernández-Ramírez and J. M. Peralta-Hernández, *Desalination*, **286**, 63 (2012).
29. A. R. Khataee, M. Zarei and A. R. Khataee, *CLEAN - Soil, Air, Water*, **39**, 482 (2011).
30. M. Moradi and F. Ghanbari, *J. Water Proc. Eng.*, **4**, 67 (2014).
31. A. K. Abdessalem, N. Oturan, N. Bellakhal, M. Dachraoui and M. A. Oturan, *Appl. Catal., B*, **78**, 334 (2008).
32. J. Yan, M. Lei, L. Zhu, M. N. Anjum, J. Zou and H. Tang, *J. Hazard. Mater.*, **186**, 1398 (2011).
33. J. Saien and A. R. Soleymani, *J. Hazard. Mater.*, **144**, 506 (2007).
34. Y.-L. Song, J.-T. Li and B. Bai, *Water, Air, Soil Pollut.*, **213**, 311 (2010).
35. D. Chakrabortty and S. S. Gupta, *J. Environ. Sci.*, **25**, 1034 (2013).
36. Y. Ding, L. Zhu, N. Wang and H. Tang, *Appl. Catal., B*, **129**, 153 (2013).
37. G. P. Anipsitakis and D. D. Dionysiou, *Environ. Sci. Technol.*, **37**, 4790 (2003).
38. N. Jaafarzadeh, F. Ghanbari and M. Moradi, *Korean J. Chem. Eng.*, **32**, 458 (2015).
39. F. Ghanbari, M. Moradi and M. Manshouri, *J. Environ. Chem. Eng.*, **2**, 1846 (2014).
40. M. Kobya and S. Delipinar, *J. Hazard. Mater.*, **154**, 1133 (2008).